Study of Carbon Black, Nitrogen and Sulphur Codoped Graphite and Graphene-Like Sheets Supported NiCo Alloy Catalyst for Hydrazine Electrooxidation in Alkaline Media

Jingyi Zhang, Jianshu Li, Chengde Huang[*]

Department of Applied Chemistry, School of Chemical Engineering and Technology,
Tianjin University, Tianjin, 300072, PR China
[*]E-mail: cdhuang@tju.edu.cn

In this work, three different types of carriers were used: VULCAN XC-72 conductive carbon black, nitrogen and sulphur codoped graphite (NSG) and the graphene-like sheets adsorbed sodium salt of flavin mononucleotide (FMNSC). Catalysts with three kinds of carriers supporting Ni and four Ni-Co alloy catalysts with different Ni-Co ratios were prepared by a simple chemical reduction method. Next, the catalytic process and performance for hydrazine electrooxidation in alkaline media were studied. The structure and morphology of the obtained Ni and Ni-Co alloy catalysts were characterized by X-ray diffraction (XRD), energy dispersive spectrometry (EDS) and X-ray photoelectron spectroscopy (XPS). The electrocatalytic performance of the catalysts toward hydrazine electrooxidation was investigated by cyclic voltammetry (CV), chronoamperometry (CA) and electrochemical impedance spectroscopy (EIS) methods. The results show that the catalytic performance of FMNSG supported NiCo with four different ratios is better than that for the conductive carbon black and nitrogen and sulphur codoped graphite. Otherwise, the catalytic performance of Ni_8Co_2 alloy catalyst is better than that of the catalysts with other Ni-Co ratios. This finding suggests that the catalytic performance can be improved by adding an appropriate proportion of Co atoms. The EIS results show that electron transfer processes present on the surface and the impedance of preliminary and secondary oxidation is also lower than for other catalysts, showing high catalytic activity. The analysis results of XPS indicate that the high amount of Ni^{2+} and Co^{2+} existed on the catalysts may be improve the rate of intermediate ($[HO–H_2N=NH_2–OH]^{2-}$) formation and rate-limiting step, thereby can enhance the electrocatalytic activity.

1. INTRODUCTION

Hydrazine (N_2H_4) is a high-energy fuel that generates environmentally friendly redox reaction (nitrogen and water) [1]. The working temperature of a hydrazine fuel cell is close to the ambient

temperature, and it has the higher power and energy density [2] than then hydrogen fuel cells, enabling its use in a wide range of applications. We think that the development of hydrazine fuel cell technology will provide the basis for its applications in the automobile industry in the future [3-5]. Therefore, it is very important to investigate hydrazine electrochemical oxidation process and mechanism [6]. While noble metals (e.g., Pt, Ag, Ru) were found to be active for hydrazine electrooxidation in alkaline media [7-8], their high cost, scarcity and instability of supply limit their applications. Transition non-noble metals and alloys (e.g., Ni, Co, Fe, Mn) were also reported to exhibit a high-performance for the electrooxidation of hydrazine hydrate in alkaline media [9-11]; these metals are inexpensive, abundant and provide stable access for the preparation of catalysts. To increases the dispersion of the catalyst and enlarge the specific surface area of the reaction, it is necessary to employed high electrical conductivity carriers for preparation the catalysts.

Very recently, nitrogen and sulphur codoped graphite (NSG) has been reported to exhibit higher electrical conductivity than the traditional carriers [12-13]. NSG exhibits an extremely low overpotential of 0.380 V to reach a current density of 10 mA cm^{-2} and shows fast kinetics with a small Tafel slope of 96 mV dec^{-1} in 0.1 M KOH for the oxygen evolution reaction (OER)[12,14]. This electrocatalytic performance is superior or comparable to those of the previously reported catalysts and shows high electrical conductivity.

Owing to its outstanding physical properties and a strong potential for application in chemistry and biology relevant technological areas, graphene is currently the focus of intense research efforts worldwide [15-18]. Coleman demonstrated that pristine graphite can be exfoliated and dispersed in solvents with surface energy matching or close to that of the basal plane of graphite (~70 mJ m^{-2}), yielding stable colloidal dispersions of single- to few-layer graphene sheets [19]. Usually, the graphene, which obtained by exfoliation of graphite, dispersions in water would be clearly advantageous, but its high surface energy implies that graphene sheets cannot be stably dispersed in water alone. Nevertheless, to change this situation, appropriate dispersants can be employed. These dispersants include ionic surfactants (e.g., sodium dodecylbenzenesulphonate and sodium cholate). nonionic/polymeric surfactants (e.g., polyvinylpyrrolidone and Pluronic copolymers) and large biomolecules (e.g., RNA and some proteins and enzymes) [19]. Dispersants should be environmentally friendly, should not degrade the material properties and should enhance graphene concentration. Unfortunately, the dispersants used so far cannot meet these requirements completely. The sodium salt of flavin mononucleotide (FMNS) has been reported to be a high-performing bio-dispersant and is an essentially non-toxic derivative of riboflavin. This material is safe enough to be a food additive. As a superior dispersant, it can stabilize graphene sheets at very high concentrations in an aqueous medium (up to ~50 mg mL^{-1}) using very low biomolecule/graphene mass ratios (~0.04) [21-22]. Furthermore, it was confirmed that using the graphite adsorbed sodium salt of flavin mononucleotide (FMNSC), graphene-noble metal (e.g., Ag，Pt，Pd) alloys which show a high catalytic activity towards the oxygen reduction reaction can be synthesized.

In this study, we focus on the Ni and Co non-noble metal elements, synthesizing Ni and four Ni-Co alloy catalysts with different Ni-Co ratios by a simple chemical reduction method. Through investigating the process of catalytic hydrazine electrooxidation in alkaline media, we compare the performance of catalysts with different Ni-Co ratios. At the same time, we vary the catalyst carriers

with three different carriers being VULCAN XC-72 conductive carbon black, nitrogen and sulphur codoped graphitee (NSG) and the graphene-like sheets adsorbed sodium salt of flavin mononucleotide (FMNSC), and we compare the catalytic performance to determine the optimal carrier.

2. EXPERIMENTAL

2.1 Experimental reagents

The carbon black (VULCAN XC-72) and carbon paper (TGP-H-090) used in this work were supplied by the Cabolt Corporation and Toray company, respectively. Nickel acetate tetrahydrate (EA, Aladdin), cobalt acetate tetrahydrate (EA, Aladdin), hydrazine (85%, Yuanli), thiourea (AR, Yuanli), sodium salt of flavin mononucleotide (93%, J&K) and graphite (99%, J&K) were used as received.

2.2 Synthesis of electrocatalysts

First, we prepared carbon black supported Ni metal (Ni/C catalyst) through a chemical reduction method. 0.30 g carbon black and 0.81 g $Ni(CH_3COO)_2·4H_2O$ salts were mixed in 50.0 mL ethylene glycol. After sonication for 20 min, the mixture was kept in a water bath of 70°C with constant mechanical stirring. Then, 10.0 mL hydrazine was added into the mixture with a constant flow pump at the flow rate of 1.0 mL min^{-1}. Then, 10.0 mL 10 M KOH solution was added into the mixture, and the Ni/C catalyst was obtained after stirring the suspension for another 15 min. After cooling down to room temperature naturally, the Ni/C catalyst was rinsed by deionized water 3–5 times, then decompressed filtered and dried in a vacuum drier [23]. The Ni/C catalyst solid powder was ground for further characterization. For the preparation of the NiCo/C alloy catalyst, a certain amount of $Co(CH_3COO)_2·4H_2O$ must be added. The molar ratios of Ni/Co in the starting materials were fixed at 10:1、9:1、8:2、7:3, and the resulting materials were named $Ni_{10}Co_1$、Ni_9Co_1、Ni_8Co_2、Ni_7Co_3.

The nitrogen and sulphur codoped graphite (NSG) was treated by hydrothermal reaction. A certain amount of oxidized graphite was added in an aqueous solution of thiourea, and then the mixture was placed into a reaction kettle heated to 180°C for 12 h. During this process, thiourea molecules were decomposed to NO_2, SO_2, and H_2O gases to react with oxidized graphite, forming nitrogen and sulphur codoped graphite (NSG) [12]. Finally, we followed the abovementioned method for loading the Ni and four different Ni-Co alloys, named Ni/NSG and NiCo/ NSG catalysts.

The procedure for the preparation of graphene-like sheets adsorbed sodium salt of flavin mononucleotide (FMNSC) was as follows: natural graphite powder was added at the concentration of 30 mg mL^{-1} to a 1 mg mL^{-1} aqueous FMNS solution and sonicated for 5 h in an ultrasound bath cleaner. After sonication, the obtained suspensions were centrifuged at 1500−2300 rpm for 20 min to sediment the unexfoliated graphite particles. The top ∼75% of the resulting supernatant was a dispersion of FMNS stabilized graphene sheets, which was collected for further use. To remove excess FMNS from the graphene dispersion, the exfoliated sheets were subjected to two cycles of sedimentation via centrifugation at 14600 rpm for 20 min and resuspension in ethylene glycol [21-22].

Finally, we followed the abovementioned method for loading the Ni and four Ni-Co alloy, with the resulting materials named Ni/FMNSC and NiCo/FMNSC catalysts.

2.3 Physical characterization

The crystallographic structures of all electrocatalysts were investigated by X-ray diffraction (XRD, Rigaku D/max 2500 V/PC, 40kV/200 mA of X-ray), 10–85°of 2θ range was tested by 4°min^{-1}. The microstructure of the as-prepared catalysts was further studied by transmission electron microscopy (TEM, JEM100CXII), the accelerating voltage was 100 kV, maximum magnification: 190,000 times times, the resolution: 0.3 nm, crystal resolution: 0.14 nm. Testing sample preparation method: dispersed the sample power in ethanol though sonication, dripped the dispersion on copper network uniformly, then drying in the air. The composition of the electrocatalysts was assessed by energy dispersive X-ray spectroscopy (EDS, Hitachi S-4800, Japan).

The crystallographic structures of all electrocatalysts were investigated by X-ray diffraction (XRD, Rigaku D/max 2500 V/PC, 40kV/200 mA of X-ray), 10–85°of 2θ range was tested by 4°min^{-1}. The composition of the electrocatalysts was assessed by energy dispersive X-ray spectroscopy (EDS, Hitachi S-4800, Japan). The surface state of the as-prepared catalysts was further studied by X-ray photoelectron spectroscopy (XPS, Kratos Axis Ultra DLD) , the X-ray source is Al K (hν= 1486.6 eV), and the charge effect of the sample surface is corrected using the C1s (284.30 eV) peak. Full spectrum scanning energy remains within the 0∼1200 eV, the pass energy is 80 eV, scanning step 1.0 eV; the narrow-spectrum scanning step is 100 meV, pass energy 40 eV, power 150 W, working voltage 15 kV, analysis area 0.7×0.3 mm^2, the vacuum of vacuum chamber vacuum 1×10^{-9} torr, resolution 0.2 eV.

2.4 Electrochemical characterization

To fabricate a working electrode, 6 mg of catalyst power was dispersed in 0.6 mL of ethanol and 20 μL of 10% PTFE solution and sonicated for 1~2 h. Next, the suspension was plated onto the TGP-H-090 carbon paper (1×1 cm^2). After being placed in the air for drying, the prepared working electrode is obtained.

The electrocatalytic activities of all electrocatalysts were measured in a conventional three-electrode system using a PAR2273 electrochemical work station. A mercuric oxide electrode (HgO, standard electrode potential 0.098 V) served as a reference electrode. The potentials were measured and reported with respect to the HgO electrode. Pt foil (area 3×3 cm^2) was used as the counter electrode, and carbon paper coated with catalyst served as the working electrode. The major electrochemical tests included cyclic voltammetry (CV), electrochemical impedance spectroscopy (EIS) and chronoamperometry (CA). The electrocatalytic oxidation of hydrazine on all electrocatalysts was measured in 1.0 mol·L^{-1} KOH +0.1 mol·L^{-1} N_2H_4·H_2O (85 wt%). The test is carried out at room temperature (25℃) without special instructions. The solution used in the test

contains alkali, which can deteriorate over a long time, so that the catalysts must be tested immediately after preparation.

CV studies were carried out at the scan rate of 20 mV s^{-1}, the potential range of -0.1−0.8 V (vs HgO), and scanning ten circles. EIS tests were conducted in the frequency range of 10 mHz to 100 kHz with a 5 mV ac amplitude; and the initial potential was the open circuit potential. The testing potential range of CA studies was from the open circuit potential to 0.55 V and the time was set to 500 s.

3. RESULTS AND DISCUSSION

Fig. 1(a)-(c) shows CV curves of the catalysts obtained during hydrazine electrooxidation. The scanning rate is 20 mV s^{-1}, the solution is 1.0 mol·L^{-1} KOH+0.1 mol·L^{-1} N$_2$H$_4$·H$_2$O and the catalysts are three kinds of carriers supporting Ni$_{10}$Co$_1$、 Ni$_9$Co$_1$、 Ni$_8$Co$_2$、 Ni$_7$Co$_3$, respectively. The ordinate current density is calculated in A/g. The positive scan process exhibited the oxidation peak (A) with the potential ranging between 0.54 V and 0.70 V. The negative scan process exhibited the reduction peak (B), with the potential ranging between 0.24 V and 0.39 V. The two strong peaks corresponded to the oxidation and reduction processes of hydrazine. Generally, the current density of the catalysts at the peak potential (0.54-0.70 V) is characterized by their catalytic activity. The peak current density of the catalysts is shown in Table 1.
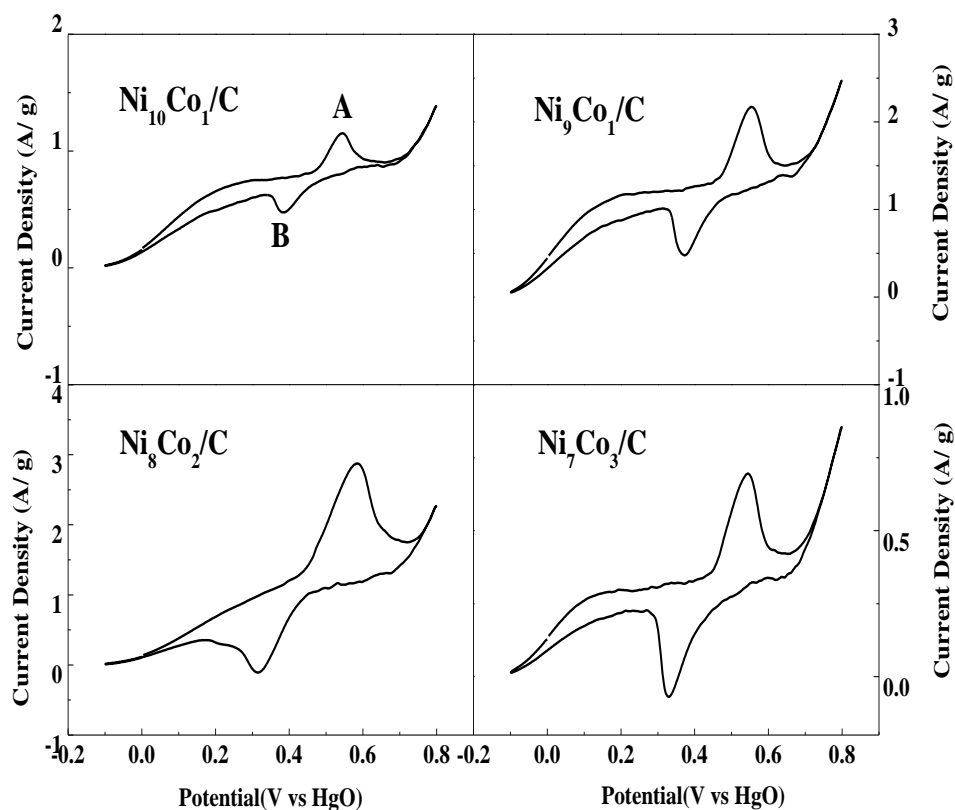
(a)
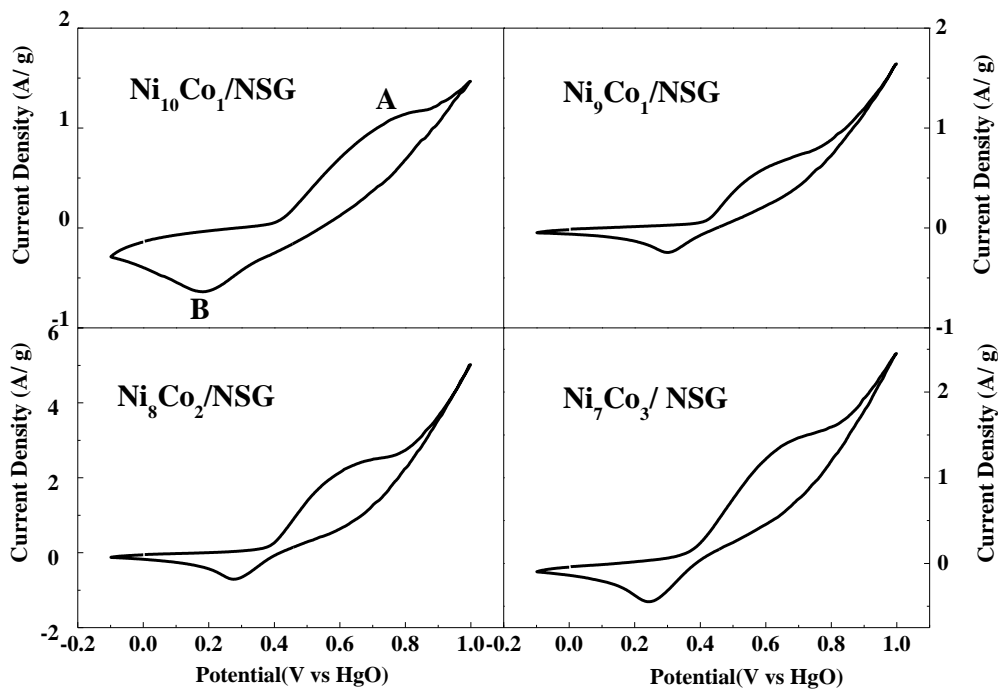
(b)
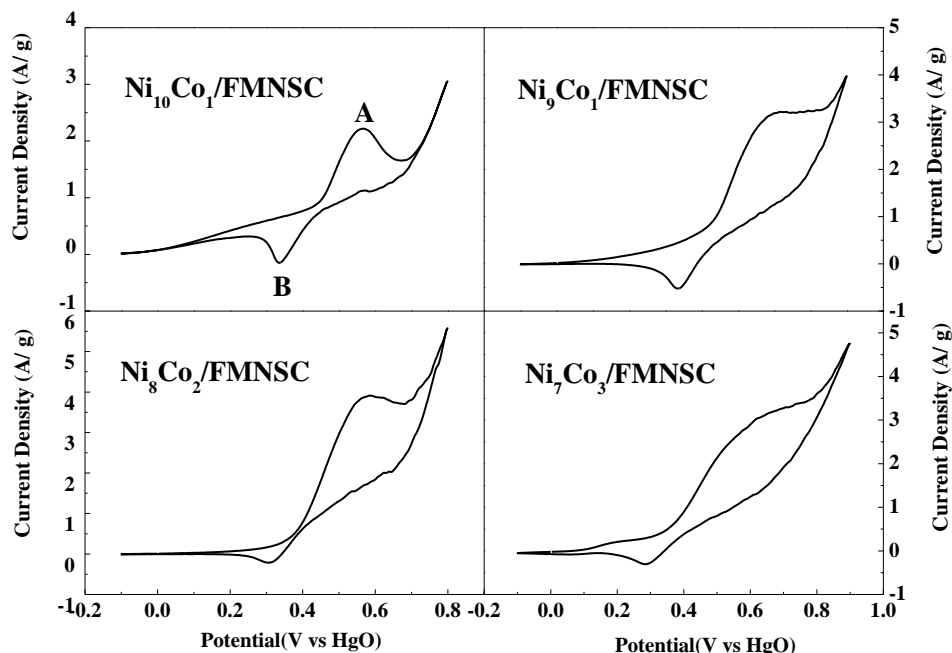
(c)

Figure 1. Cyclic voltammograms of the prepared catalysts at scan rate of 20 mV s^{-1} in 1 mol/L KOH+0.1 mol/L N$_2$H$_4$·H$_2$O solution under room temperature

Comparison of the peak current density values shows that the catalytic activity for all ratios of NiCo/FMNSC is better than for the other catalysts. Furthermore, the peak current density value of Ni$_8$Co$_2$/FMNSC is the highest. This suggests that the catalytic performance of Ni$_8$Co$_2$/FMNSC is the best.

Table 1. Catalytic activities towards the hydrazine oxidation of catalysts

| Electrocatalyst	Current density for A peak $I/A\cdot g^{-1}$	Electrocatalyst	Current density for A peak $I/A\cdot g^{-1}$
$Ni_{10}Co_1/C$	1.14	Ni_8Co_2/NSG	2.54
Ni_9Co_1/C	2.18	Ni_7Co_3/NSG	1.49
Ni_8Co_2/C	2.85	$Ni_{10}Co_1/FMNSC$	2.26
Ni_7Co_3/C	0.69	$Ni_9Co_1/FMNSC$	3.20
$Ni_{10}Co_1/NSG$	1.12	$Ni_8Co_2/FMNSC$	3.86
Ni_9Co_1/NSG	0.69	$Ni_7Co_3/FMNSC$	3.25

We compared the CV results with other electrocatalysts for hydrazine electrooxidation. Table 2 shows a remarkable electrocatalytic activity toward the oxidation of hydrazine compared to previous studies. From the table 2, it can be seen that $Ni_8Co_2/FMNSC$ catalyst has a relative high current density for hydrazine oxidation peak. It is evident that $Ni_8Co_2/FMNSC$ catalyst has a good catalytic activity [29]. Compare to Pt/Graphiene-Oxide [24], $Ni_8Co_2/FMNSC$ have some advantages, such as low cost and high electrochemical activity. Of course, the current density value of $Ni_8Co_2/FMNSC$ catalyst is not the highest one. It may be the reason that we cannot spray more catalyst powder on the electrodes which is only 6mg. What's more, it's may be other reason that we didn't use rotating disk electrode system. And it is believed that the high electrocatalytic activity of as-prepared $Ni_8Co_2/FMNSC$ not only relies on the Ni/Co ratio but also highly relates to the use graphene-like carbon materials as support.

Table 2. Cyclic voltammograms results comparison of the catalysts for hydrazine oxidation with reported results.

Electrocatalyst	Current density for oxidation peak (mA/cm^2)	solution	scan rate (mV/s)	Ref.
Graphene oxide-Pt(Pt/GO)	4	$H_2SO_4+ N_2H_4\cdot H_2O$	25	[24]
Co/ carbon fiber cloth(Co/CFC)	30	$KOH+ N_2H_4\cdot H_2O$	20	[25]
Smooth electroless NiCuP amorphous plating(SA-NiCuP)	4.43	$KOH+ N_2H_4\cdot H_2O$	50	[26]
Nanoporous NiCu crystalline alloy (NP-NiCu)	6.30	$KOH+ N_2H_4\cdot H_2O$	50	[26]
Zeolite-encapsulated Ni(II)(salen) complex supported on graphite modified glassy carbon electrode (Ni(II)(salen)Y/GCE)	19	$KOH+ N_2H_4\cdot H_2O$	20	[27]
Ceria nanoparticles grown on reduced graphene oxide (CeO_2/RGO)	20	$KOH+ N_2H_4\cdot H_2O$	20	[28]
NiCuCo/ Graphene	53	$KOH+ N_2H_4\cdot H_2O$	100	[29]
$Ni_8Co_2/FMNSC$	23.16	$KOH+ N_2H_4\cdot H_2O$	20	This work

*The results calculated according to the information reported in related papers.

The performance of all electrocatalysts was also tested by chronoamperometry (CA). The short-time current density at the constant potential of 0.55 V (vs. HgO) in 1.0 mol·L^{-1} KOH+0.1 mol·L^{-1} N$_2$H$_4$·H$_2$O solution is shown in Figs. 2(a)-(c). During the initial stages of oxidation, the potentiostatic current density of all electrocatalysts consistent with the CV results decreased rapidly, which may be attributed to the formation of intermediate species[30]. The oxidation current first decreased and then finally reached a stable state. It can be observed that the catalysts with FMNSC carriers showed the fastest stabilization, and the stable current density of Ni$_8$Co$_2$ was the largest in the three kinds of carrier catalysts. The stable current density of hydrazine electro-oxidation followed the order Ni$_8$Co$_2$/FMNSC＞Ni$_8$Co$_2$/C＞Ni$_8$Co$_2$/NSG, which is in agreement with the CV results.
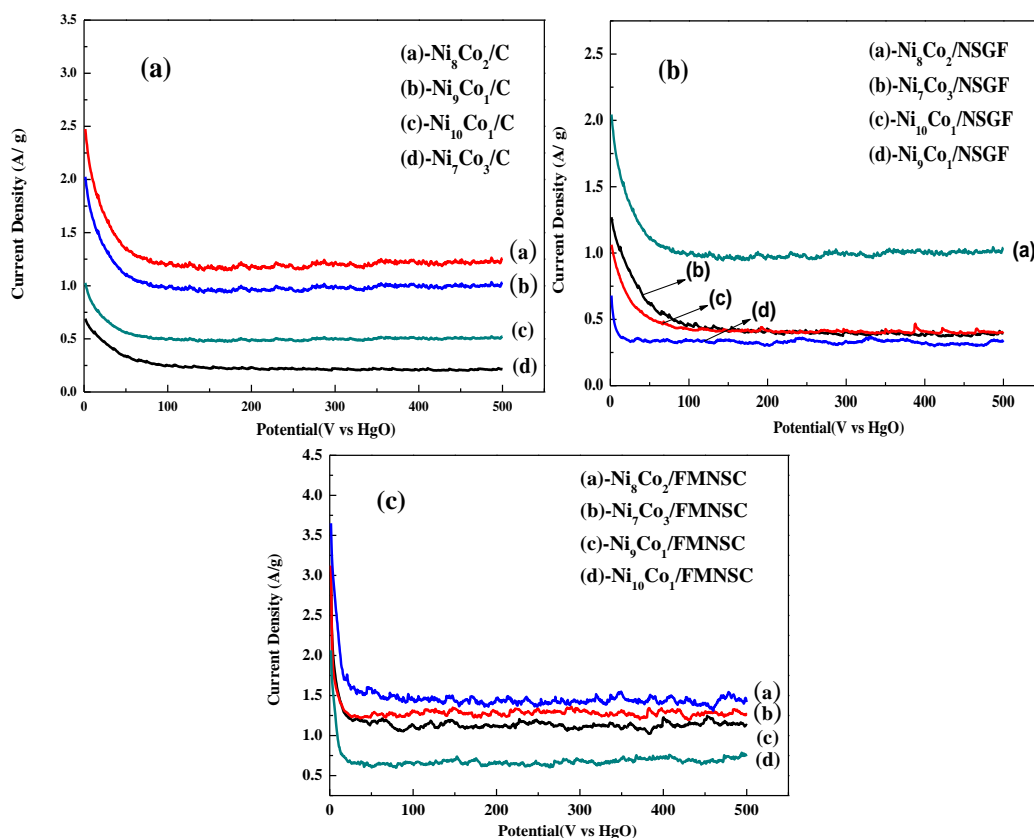

Figure 2. Current density-time plots of the prepared catalysts in 1mol/L KOH+0.1mol/L N$_2$H$_4$·H$_2$O at 0.55V vs. HgO at room temperature

In order to understand the reasons of the origin of the catalytic activity improvement of the FMNSC carriers supported catalysts, the physicochemical and chemical properties of the catalysts are characterized.

The XRD patterns of the prepared Ni/C and four NiCo/C catalysts are presented in Fig. 3(a), and those of the prepared Ni/FMNSC and four NiCo/ FMNSC catalysts are presented in Fig. 3(b). A

broad diffraction peak can be observed at 25° in Fig. 3(a), which is the characteristic peak of Vulcan XC-72 (PDF#75-1621). The peaks at 26.5° and 55° in Fig. 3(b) are assigned to the diffraction of natural graphite (002) and (004) planes, respectively. These diffraction peaks at approximately 2θ=44.5°, 51.8° and 76.4° of Ni/C in Fig. 3(a) and Ni/FMNSC in Fig. 3(b) were indexed to the (111), (200) and (220) crystalline plane diffraction of face-centred cubic Ni (PDF#04-0850) [31-32]. The 2θ of all NiCo alloy shows a distance shift relative to the Ni standard.
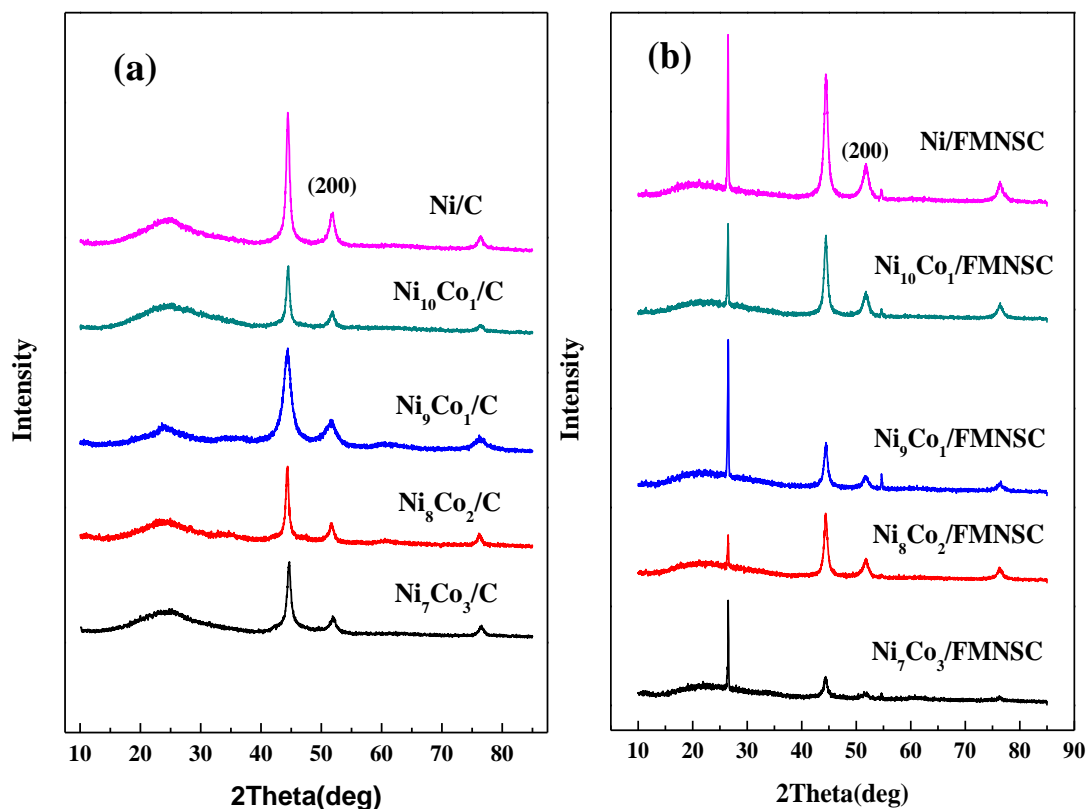
**Figure 3.** XRD pattern of the prepared catalysts at the range of 10-85˚

Table 3. The analysis of XRD patterns

Electrocatalyst	Particle Size	Electrocatalyst	Particle Size
Ni/C	12.5nm	Ni/FMNSC	12.4nm
$Ni_{10}Co_1$/C	14.4nm	$Ni_{10}Co_1$/FMNSC	13.9nm
Ni_9Co_1/C	13.8nm	Ni_9Co_1/FMNSC	12.6nm
Ni_8Co_2/C	14.9nm	Ni_8Co_2/FMNSC	11.8nm
Ni_7Co_3/C	14.9nm	Ni_7Co_3/FMNSC	11.1nm

This indicates that when Ni and Co form an alloy, they will interact with each other [33]. Ni (200) diffraction peak was used to estimate the average size of the catalysts by the Scherrer equation, $D=0.89\lambda/Bcos\theta$ (D is the average size of the catalysts in nm, λ=0.154056 nm is the X-ray wavelength,

B is the full width at half-maximum in radians, and θ is the diffraction angle at peak position). The results showing the size of Ni particles in the catalysts are present in Table 3. Examination of the data presented in Table 3 shows that the size of Ni particles in NiCo/FMNSC was smaller than that in NiCo/C. In general, the small grain size indicates that the catalyst has a large reaction surface area and is beneficial for the improvement of the catalytic activity. Therefore, we believe that the grain size is small for the catalysts prepared using FMNSC. This is one of the reasons for the improved catalytic performance of this catalyst.

Fig. 4(a) presented the TEM images of the prepared Ni_8Co_2/C catalysts, and Fig. 4(b) were $Ni_8Co_2/FMNSC$ catalysts. As shown in Fig.4, VULCAN XC-72 is spherical shape, and FMNSC likes sheets.
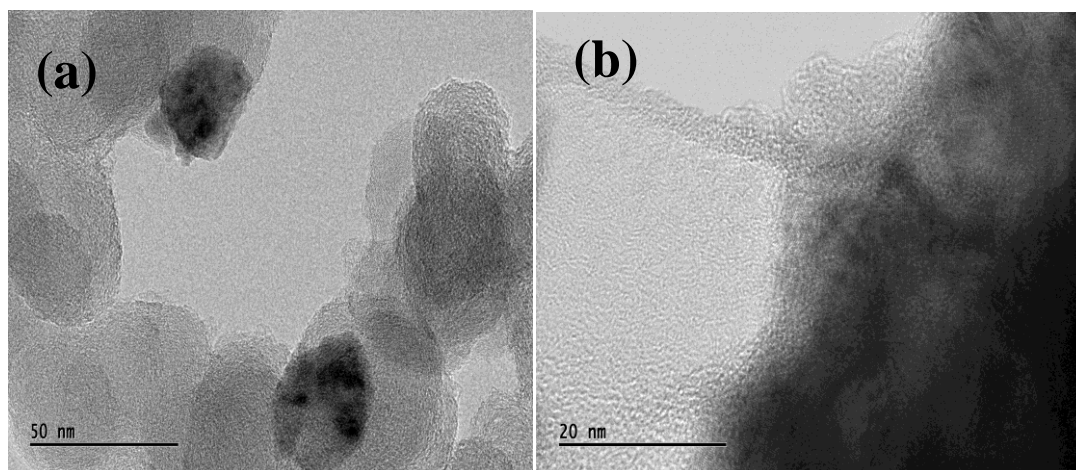
**Figure 4.** TEM images of the prepared catalysts Ni_8Co_2/C (a), and $Ni_8Co_2/FMNSC$ (b)

Table 4. The content and atomic ratio of element according to the EDS spectra

Sample	C wt%	Ni wt%	Co wt%	NiCo at%
Ni/C	63.92	36.08	--	--
Ni/NSGF	52.48	41.51	--	--
Ni/FMNSC	44.84	55.16	--	--
NiCo/C 8:2	77.41	18.26	4.34	8:1.75
NiCo/NSGF 8:2	19.08	57.98	14.73	8:2.02
NiCo/FMNSC 8:2	20.98	63.98	15.04	8:1.88

To study the types and content of the elements in the catalysts, EDS measurements were performed. The EDS results were tabulated in Table 4. The data in Table 4 show the presence of Ni and Co, and the amounts of Ni and Co particles of the FMNSC catalysts increase obviously. We suggest that the surface structure of FMNSC carriers is better than that of the other catalysts, with more binding sites available for the loading of the Ni and Co particles. Thus, the amounts of Ni and Co particles increase gradually. The presence of Ni, Co and C were observed in Table 4. This indicates

that the hydrazine can reduce both Ni^{2+} and Co^{2+}. We can see that the final molar ratio of Ni-Co is 8:1.75，8:2.02，8:1.88, close to the initial molar ratio. This indicates that the hydrazine reduces Ni^{2+} and Co^{2+} to the same degree.

Figs. 5(a)-(b) show the XPS images obtained for the $Ni2p_{3/2}$ 和 $Co2p_{3/2}$ of Ni_8Co_2/C, and Figs. 5(c)-(d) show the XPS images obtained for the $Ni2p_{3/2}$ 和 $Co2p_{3/2}$ of $Ni_8Co_2/FMNSC$, with the analysis data listed in Table 5. In general, Ni $2p_{3/2}$ and Ni $2p_{1/2}$, Co $2p_{3/2}$ and Co $2p_{1/2}$ appear at the same time. According to the report of Ma [34], a fitting analysis is performed only for Ni $2p_{3/2}$ and Co $2p_{3/2}$. Examination of Figs. 5(a) and 5(c) shows that there are five fitting peaks for Ni $2p_{3/2}$: the binding energy between 851.6-852.2eV corresponds to Ni^0, and the binding energy between 852.8-856.9eV corresponds to Ni^{2+} and the satellite peaks. According to the relevant reports, the Ni^{2+} should be due to NiO 和 Ni $(OH)_2$[35-36]. Examination of Figs. 5(b) and 5(d) shows that there are four fitting peaks for Co $2p_{3/2}$: the binding energy between 778.1-778.7eV corresponds to Co^0, and the binding energy between 778.1-783.6eV corresponds to Co^{2+} and the satellite peaks. According to the reported of Fernandes[35], the Co^{2+} should be due to CoO and Co$(OH)_2$.
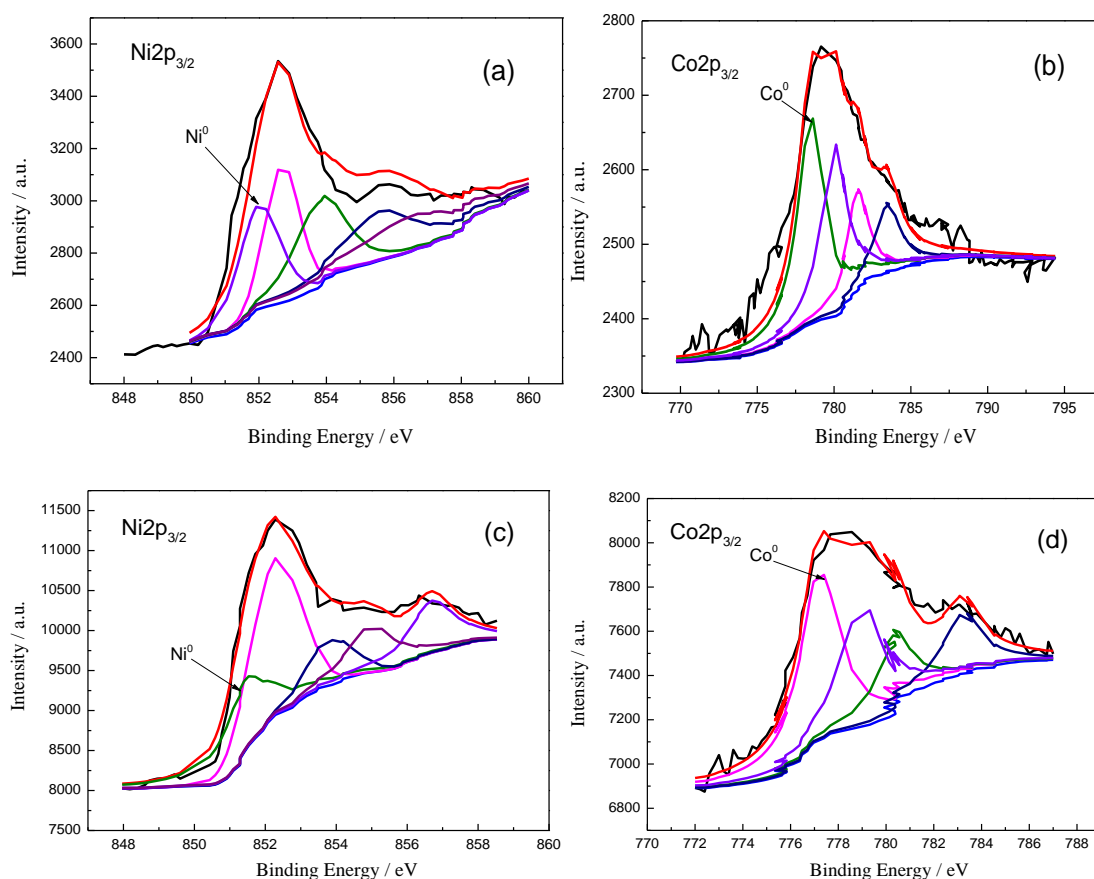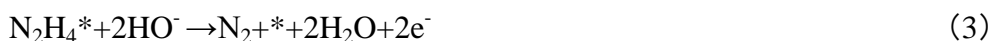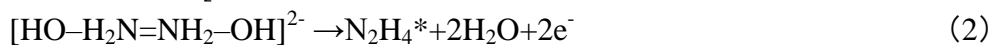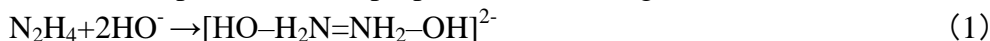

Figure 5. The fitting results of Ni $2p_{3/2}$ and Co $2p_{3/2}$ XPS spectrum for Ni_8Co_2/C (a, b) and $Ni_8Co_2/FMNSC$(c, d)

Table 5. Ni $2p_{3/2}$ and Co $2p_{3/2}$ deconvoluted XPS spectra of the studied samples

| Catalyst	Peak	Species	Binding Energy (eV)	Relative Ratio(%)
Ni_8Co_2/C	Ni $2p_{3/2}$	Ni^0	852.2	36.71
		Ni^{2+}	852.8，854 856.7，855.8	63.29
	Co $2p_{3/2}$	Co^0	778.7	41.68
		Co^{2+}	780.2，781.7 783.6	58.32
Ni_8Co_2/ FMNSC	Ni $2p_{3/2}$	Ni^0	851.6	19.65
		Ni^{2+}	854，852.5 856.9，855.2	80.35
	Co $2p_{3/2}$	Co^0	778.1	40.30
		Co^{2+}	780.5，781.6 783.4	59.70

Based on the view of Karim-Nezhad and co-workers [38], Y. Ma [34], V. Rosca [39]. We know the first intermediate of hydrazine oxidation in alkaline solution was $[HO–H_2N=NH_2–OH]^{2-}$. The hydrazine oxidation process can be proposed as following [34,38-39]:

$$N_2H_4+2HO^- \rightarrow [HO–H_2N=NH_2–OH]^{2-} \tag{1}$$
$$[HO–H_2N=NH_2–OH]^{2-} \rightarrow N_2H_4*+2H_2O+2e^- \tag{2}$$
$$N_2H_4*+2HO^- \rightarrow N_2+*+2H_2O+2e^- \tag{3}$$

N_2H_4 combine with OH^- to first generate intermediate products $[HO–H_2N=NH_2–OH]^{2-}$(this step is the rate-limiting step), then the intermediate product carries out two two-electron transfer processes, finally completing the entire oxidation process. From Table 5 we can see that the contents of the Ni^0 and Co^0 in the catalyst Ni_8Co_2/FMNSC was lower than that in Ni_8Co_2/C. This shows that the high metal content on the catalyst surface is unfavourable for the hydrazine oxidation process. Owing to the presence of Ni^{2+} and Co^{2+}, it is possible to increase the OH^- content of the catalyst surface, which will increase the generating rate of the intermediate product in the rate-limiting step. Therefore, the increased Ni^{2+} and Co^{2+} content may be another important reason for the better hydrazine electrooxidation catalytic activity of Ni_8Co_2/FMNSC relative Ni_8Co_2/C.

Considering the CV and CA results described above, the Ni_8Co_2 catalysts exhibited good catalytic activity, so we further tested the EIS. The Nyquist plot is shown in Fig. 6. From the magnified figure in Fig. 6, the semicircle whose angles drift off horizontal line of Ni_8Co_2/ FMNSC is approximately 45°, including the diffusion process. Based on the reaction steps of the hydrazine electrochemical oxidation described in the aforementioned report by Ma[34], we believe that the process may contain two time parameters. Therefore, we used Fig. 7(b) to fit the Nyquist plot. Otherwise, the Ni_8Co_2/C image shows that there is no diffusion control. We therefore used Fig. 7(a) to fit the Nyquist plot. The values of the elements in the equivalent circuit are presented in Table 6. In the equivalent electric circuit, the R_{sol} consist of the solution resistance (between the Luggin capillary and electrode) and contact resistance. The varied diameters of these semicircles indicated different charge

transfer resistances [40]. Table 6 shows that the R_{sol} values for the three kinds of carrier catalysts range from 3.447 to 3.494 $\Omega \cdot cm^{-2}$, showing little difference. According to the mechanism analysis discussed above, the oxidation process is divided into two steps, including the initial oxidation (equation 2 $[HO–H_2N=NH_2–OH]^{2-} \rightarrow N_2H_4*+2H_2O+2e^-$) and the secondary oxidation (equation 3 $N_2H_4*+2HO^- \rightarrow N_2+*+2H_2O+2e^-$). Q1 and R_1 represent the constant phase angle element and charge transfer resistance during the initial oxidation process. Similarly, Q_2 and R_2 represent the constant phase angle element and charge transfer resistance during the secondary oxidation process. As is evident from the inspection of the data in Table 6, both the R_1 and R_2 of $Ni_8Co_2/$ FMNSC were smaller the those for the other two catalysts, and we can infer that the resistance values of the two oxidation processes were the smallest, which is agreement with the CV and CA results.
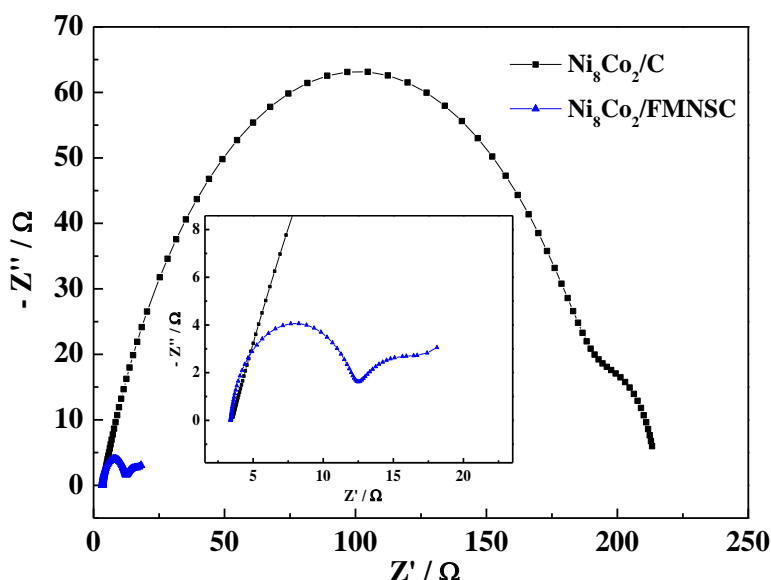
Figure 6. EIS of catalysts Ni_8Co_2/C, $Nki_8Co_2/FMNSC$ in 1mol/L KOH+0.1mol/L $N_2H_4 \cdot H_2O$ at open-circuit potential under room temperature Nyquist plots
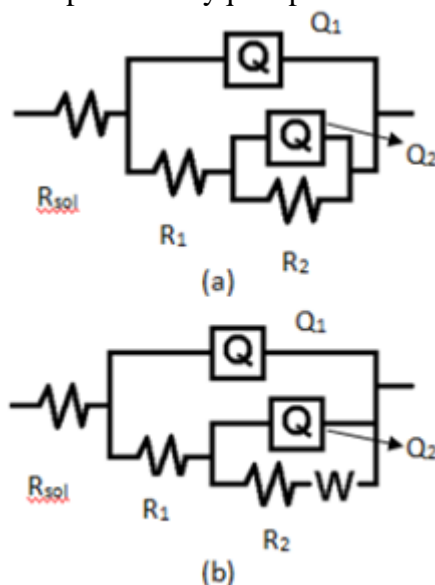
Figure 7. (a) is the equivalent circuit of EIS spectra for Ni_8Co_2/C; (b) is the equivalent circuit of EIS spectra for $Ni_8Co_2/$ FMNSC.

Furthermore, comparing the R_1 and R_2 of all catalysts, we can see that the charge transfer resistance during the secondary oxidation process was smaller than that during the initial oxidation process. Based on the above analysis, we can infer that the secondary oxidation process was easier than the initial oxidation process. This may be due to the compound adsorbing the intermediate during initial oxidation process, which then made the secondary oxidation process reaction proceeds more easily.

Table 6. The values of the elements in equivalent circuit in Figure 7

Electrocatalyst	R_{sol} $\Omega \cdot cm^{-2}$	$Q_1 \times 10^{-4}$ $F \cdot cm^{-2}$	R_1 $\Omega \cdot cm^{-2}$	$Q_2 \times 10^{-4}$ $F \cdot cm^{-2}$	R_2 $\Omega \cdot cm^{-2}$	W $\Omega \cdot cm^{-2}$
Ni_8Co_2/C	3.494	3.666	94.8	1187	57.12	--
$Ni_8Co_2/FMNSC$	3.447	22.59	34.82	56.87	17.26	24.92

4. CONCLUSIONS

In this work, we used catalysts with three types of carriers supporting Ni and four Ni-Co alloys that were prepared by a simple chemical reduction method. The three different kinds of carriers are VULCAN XC-72 conductive carbon black, nitrogen and sulphur codoped graphite (NSG) and the graphene-like sheets adsorbed sodium salt of flavin mononucleotide (FMNSG). Then, we studied the catalytic process and performance for hydrazine electrooxidation in alkaline media, and the catalysts were characterized by physical and chemical tests. The following conclusions were obtained: (1) different carriers have important influence on the catalytic activity. The three kinds of carriers supported catalysts including conductive carbon black, NSG and FMNSC show different catalytic activities in the electrocatalytic oxidation of hydrazine. From the peak current density in CV plots and the images of CA, it is known that the catalytic activity is better when FMNSC is used as the carrier than when conductive carbon black and NSG carriers are. (2) There is a certain influence on the catalytic performance of the catalysts with different Ni_8Co_2 alloy ratios. The catalytic performance of the Ni_8Co_2 alloy catalyst is better than that for other ratios. This suggests that the catalytic performance can be improved by adding an appropriate proportion of Co atoms. (3) Through XRD, XPS and EIS analyses, it can be concluded that owing to the small grain size of Ni_8Co_2 in $Ni_8Co_2/FMNSC$ and the abundance of Ni^{2+} and Co^{2+} on the surface of the catalyst with FMNSC as the carrier, the reaction surface area of the catalyst is enhanced and the generating rate of intermediate product[HO–$H_2N=NH_2$–OH]$^{2-}$ is accelerated. Consequently, the two times transfer resistance is reduced and the catalytic activity is improved.

References

1. Y. Ma, H. Li, R. Wang R, H. Wang, W. Lv, S. Ji, *J. Power Sources*., 289 (2015) 22.

2. F. Jia, J. Zhao, X. Yu, *J. Power Sources*, 222(2013) 135.
3. K. Yamada, K.Yasuda, N. Fujiwara, Z. Siroma, H. Tanaka, Y. Miyazaki, T. Kobayashi, *Electrochem. Commun.*, 5 (2003) 892.
4. W. X. Yin, Z. P. Li, J. K. Zhu, H. Y. Qin, *J. Power Sources*, 182 (2008) 520.
5. A. Serov, C, Kwak, *Appl. Catal. B: Environ.*, 98 (2010) 1.
6. Z. Lu, M. Sun, T. Xu, Y. Li, W. Xu, Z. Chang, Y. Ding, X. Sun, L. Jiang, *Adv. Mater.*, 27 (2015) 2361.
7. K. Kořínek, J. Koryta, M. Musilova, *J. Electroanal. Chem. Interfac.*, 21 (1969) 319.
8. B. Dong, B. L. He, J. Huang J, G. Y. Gao, Z. Yang, H. L, Li, *J. Power Sources*, 175 (2008) 266.
9. B. Filanovsky, E. Granot, I. Presman I, I. Kuras, F. Patolsky, *J. Power Sources*, 246 (2014) 423.
10. M. Gong, H. Dai, *Nano Res.*, 8 (2015) 23.
11. X. Yu, M. Zhang, W. Yuan, G. Shi, *J. Mater. Chem.*, 3 (2015) 6921.
12. X. Yu, M. Zhang, J. Chen, Y. Li, G. Shi, *Adv. Energy Mater.*, 6 (2016) 1501492.
13. X. X. Ma, Y. Su, X. Q. He, *Catal. Sci. Technol.*, 7 (2017) 1181.
14. Y Su, Y. Zhang, X. Zhuang, S. Li, D. Wu, F. Zhang, X. Feng, *Carbon.*, 62 (2013) 296.
15. A.K. Geim, *Science*, 324 (2009) 1530.
16. K.S. Novoselov, V.I. Falko, L. Colombo, P.R. Gellert, M.G. Schwab, K. Kim, *Nature*, 490 (2012) 192.
17. J. Wang, Z. Dong, J. Huang, J. Li, X. Jin, J. Niu, J. Sun, J. Jin, J. Ma, *Appl. Surf. Sci.*, 270 (2013) 128.
18. S. Stankovich, D. A. Dikin, G. H. B. Dommett, K. M. Kohlhaas, E. J. Zimney, E. A. Stach, R. D. Piner, S. T. Nguyen, R. S. Ruoff, *Nature*, 442 (2006) 282.
19. W. Yoon, Y. Lee, H. Jang, M. Jang, J. S. Kim, H, S. Lee, S. Im, D. W. Boo, J. Park, S. Y. Ju, *Carbon*, 81 (2015) 629.
20. S. Y. Ju, D. C. Abanulo, C. A. Badalucco, C. A. Badalucco, J. A. Gascón, F. Papadimitrakopoulos, *J. Am. Chem. Soc.*, 134 (2012) 13196.
21. A. Abellán-Llobregat, M. Ayán-Varela, L. Vidal, J. I. Paredes, S. Villar-Rodil, A. Canals, E. Morallón, *J. Electroanal. Chem.*, 783 (2016) 41.
22. M. Ayán-Varela, J. I. Paredes, L. Guardia, S. Villar-Rodil, J. M. Munuera, M. Díaz-González, C. Fernández-Sánchez, A. Martínez-Alonso, J. M. D. Tascón, *ACS Appl. Mater. Interfaces.*, 7 (2015) 10293.
23. S. Lu, D. Cao, X. Xu, H. Wang, Y. Xiang, *RSC Advances.,* 4 (2014) 26940.
24. J. D. Kim, M. Y. Choi, H. C. Choi, *Applied Surface Science.*, 420(2017) 700.
25. R. Liu, X. Jiang, F. Guo, *Electrochimica Acta.*, 94(2013) 214.
26. X. L. Wang, Y. X. Zheng, M. L. Jia, *International Journal of Hydrogen Energy.*, 41(2016), 8449.
27. R. Zhang, L. Liu, Y. Li, *Int. J. Electrochem. Sci.*, 10(2015) 2355.
28. M. Srivastava, A. K. Das, P. Khanra, M. E. Uddin, N. H. Kima, J. H. Lee, *J. Mater. Chem. A.*, 1 (2013) 9792.
29. M. Jafarian, T. Rostami, M. G. Mahjani, *Journal of Electroanalytical Chemistry.*, 763 (2016) 134.
30. S. R. Hosseini, M. Kamali-Rousta, *Electrochimica Acta.,* 189(2016) 45.
31. J. Sanabria-Chinchilla, K. Asazawa, T. Sakamoto, K. Yamada, H. Tanaka, P. Strasser, *J. Am. Chem. Soc.*, 133 (2011) 5425.
32. X. Liu, Y. Li, N. Chen, *Electrochimica Acta.*, 213(2016)730.
33. Y. Zhu, Z. Li, C. Huang, *Electrochimica Acta.*, 153(2015)439.
34. Y. Ma, H. Wang, W. Lv, S. Ji, B. G. Pollet, S. Li, R. Wang, *RSC Advances.*, 5 (2015) 68655.
35. R. Fernandes, N. Patel, A. Miotello, M. Filippi, *J. Mol. Catal. A Chem.*, 298 (2009) 1.
36. X. P. Wen, H. B. Dai, L. S. Wu, *Applied Surface Science.*, 409(2017)132.
37. B. Zhao, Y. W. Chen, *J. Non-Cryst. Solids.*, 356 (2010) 839.
38. G. Karim-Nezhad, R. Jafarloo, P. S. Dorraji, *Electrochim. Acta.*, 54 (2009) 5712.
39. V. Rosca, M. T. M. Koper, *Electrochimica Acta.*, 53(2008)5199.

40. M. Sun, Z. Lu, L. Luo, *Nanoscale*., 8(2016)1479.